

# The Character and Formation of Elongated Depressions

## on the Upper Bulgarian Slope

XU Cuiling<sup>1,2</sup>, GREINERT Jens<sup>2\*</sup>, HAECKEL Matthias<sup>2</sup>, BIALAS Jörg<sup>2</sup>, DIMITROV Lyubomir<sup>3</sup>, ZHAO Guangtao<sup>1</sup>

1) College of Marine Geo-Sciences, Ocean University of China, Qingdao 266100, China

2) GEOMAR Helmholtz Centre for Ocean Research Kiel, Kiel 24148, Germany

3) Institute of Oceanology Bulgarian Academy of Science, Varna 9000, Bulgaria

**Abstract** Seafloor elongated depressions are indicators of gas seepage or slope instability. Here we report a sequence of slope-parallel elongated depressions that link to headwalls of sediment slides on upper slope. The depressions of about 250 m in width and several kilometers in length are areas of focused gas discharge indicated by bubble-release into the water column and methane enriched pore waters. Sparker seismic profiles running perpendicular and parallel to the coast, show gas migration pathways and trapped gas underneath these depressions with bright spots and seismic blanking. The data indicate that upward gas migration is the initial reason for fracturing sedimentary layers. In the top sediment where two young stages of landslides can be detected, the slope-parallel sediment weakening lengthens and deepens the surficial fractures, creating the elongated depressions in the seafloor supported by sediment erosion due to slope-parallel water currents.

**Keywords:** methane seepage, elongated depression, pockmark, landslide, Black Sea

### 1. Introduction

Seafloor elongated depressions, indicators for gas seepage or slope instability, have been reported from several continental margins, such as the West African margin, the Turkish Black Sea shelf, the mid-U.S. Atlantic coast, the Norwegian continental slope and the Santa Barbara Basin (Pilcher and Argent, 2007; Çifçi et al., 2003; Driscoll et al., 2000; Newman et al., 2008; Mienert et al., 2010; Reiche et al., 2011; Laberg et al., 2013; Greene et al., 2006).

---

\* GREINERT Jens  
Email: [jgreinert@geomar.de](mailto:jgreinert@geomar.de)  
Tel.: +49 431 600-2590

30 Two explanations are given for their formation mechanisms. One is linked to submarine gas  
31 release from “pockmarks” that are grouped together (Hovland et al., 2002; Bøe et al., 1998;  
32 Pilcher and Argent, 2007; Hill et al., 2004), the other is that they are opening tensional  
33 “cracks” as a result of slope instability. In the latter explanation they are regarded as the initial  
34 stage of a landslide (Laberg et al., 2013; Reiche et al., 2011; Martel, 2004; Greene et al.,  
35 2006).

36 On continental slopes, elongated depressions are often associated with both mass movement  
37 and gas seepage. So the initial reason for their occurrence is controversially discussed. Çifçi et  
38 al. (2003), Hill et al. (2004) and Mienert et al. (2010) proposed that elongated depressions are  
39 created by gas seepage. In contrast, Driscoll et al. (2000), Martel (2004), Greene et al. (2006)  
40 and Reiche et al. (2011) suggested that in their study areas the elongated depressions are  
41 mainly a result of slope instability related to surrounding landslides or are influenced by older  
42 landslides further downslope. In our paper we discuss whether one of the two processes, gas  
43 seepage or sediment movement, is the main driver for the elongated depressions on the upper  
44 slope offshore southern Bulgaria, Black Sea.

45 Multibeam echosounder (MBES) data recorded during SPUX cruise with RV Akademik in  
46 2012 show formerly reported ‘pockmarks’ (Dimitrov and Dontcheva, 1994) to be actually  
47 elongated depressions. Current and past gas seepage zones as well as different stages of  
48 landslides are identified by combining geological, geophysical and geochemical studies. We  
49 present the distribution and shape of the elongated depressions as well as their sub-surface  
50 structure to discuss the possible relationship between the elongated depressions and mass  
51 movement or gas seepage.

52

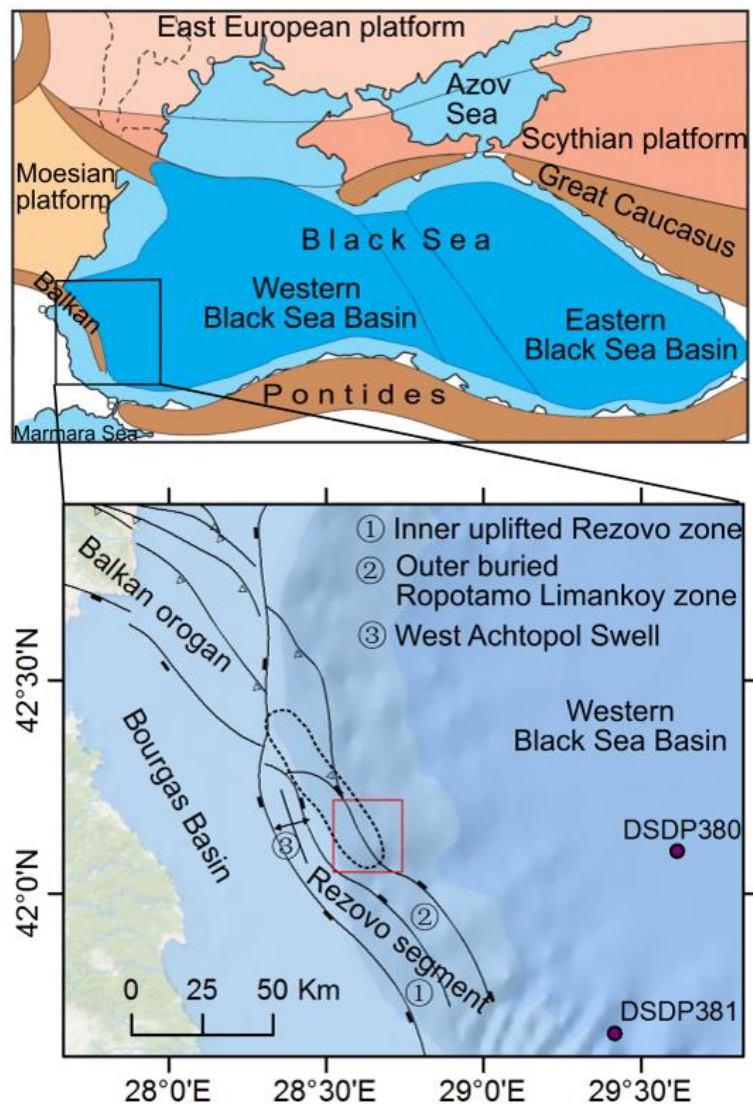
## 53 **2 Geological setting**

54 The Western Black Sea Basin (WBSB) is a back-arc basin that developed north of the Pontide  
55 Magmatic Arc as a consequence of the northward subduction of the Neo-Tethys oceanic plate.  
56 The study area is located on the submarine prolongation of the Balkan Orogen ( Fig. 1;  
57 Georgiev, 2012). To the west the anticlinal structure of the West Achtopol Swell affects the  
58 Mid-Quaternary strata (Dimitrov and Dontcheva, 1994; Genov and Dimitrov, 2003).

59 The thickness of the overlying sedimentary strata on the basement increases seaward, from  
60 about 1.5 km at the upper slope to 3-3.5 km in the WBSB (Georgiev, 2012). The thickness of  
61 Quaternary sediments is more than 600 m at the slope base just seaward of the study area  
62 (Dimitrov and Dontcheva, 1994). Affected by global sea level change during the Quaternary,

63 the sedimentary environment of the Black Sea alternated between a saline sea and a fresh  
 64 water lake (Ross, 1974). The superficial Holocene layers are silty clay enriched in organic  
 65 matter ( $C_{org}$  1-5 %) with a thickness of typically 2 m, but the underlying Upper Pleistocene  
 66 sediments are lacustrine clayey mud with  $C_{org}$  concentrations of less than 1 %.

67 The pockmark zone reported by Dimitrov and Dontcheva (1994) is located at the shelf edge,  
 68 while the southern part, resurveyed during the SPUX cruise, is located in the upper part of the  
 69 continental slope. The pockmark zone is bounded by the Rezovo fault to the south. The  
 70 northern bounding cannot be determined due to lack of data.



71

72 Fig. 1 Main structural features of the Bulgarian Black Sea zone (Georgiev, 2012). The study  
 73 area is marked by red rectangle, the pockmark zone reported by Dimitrov and Dontcheva,  
 74 (1994) are marked by dash line.

### 75 **3. Materials and methods**

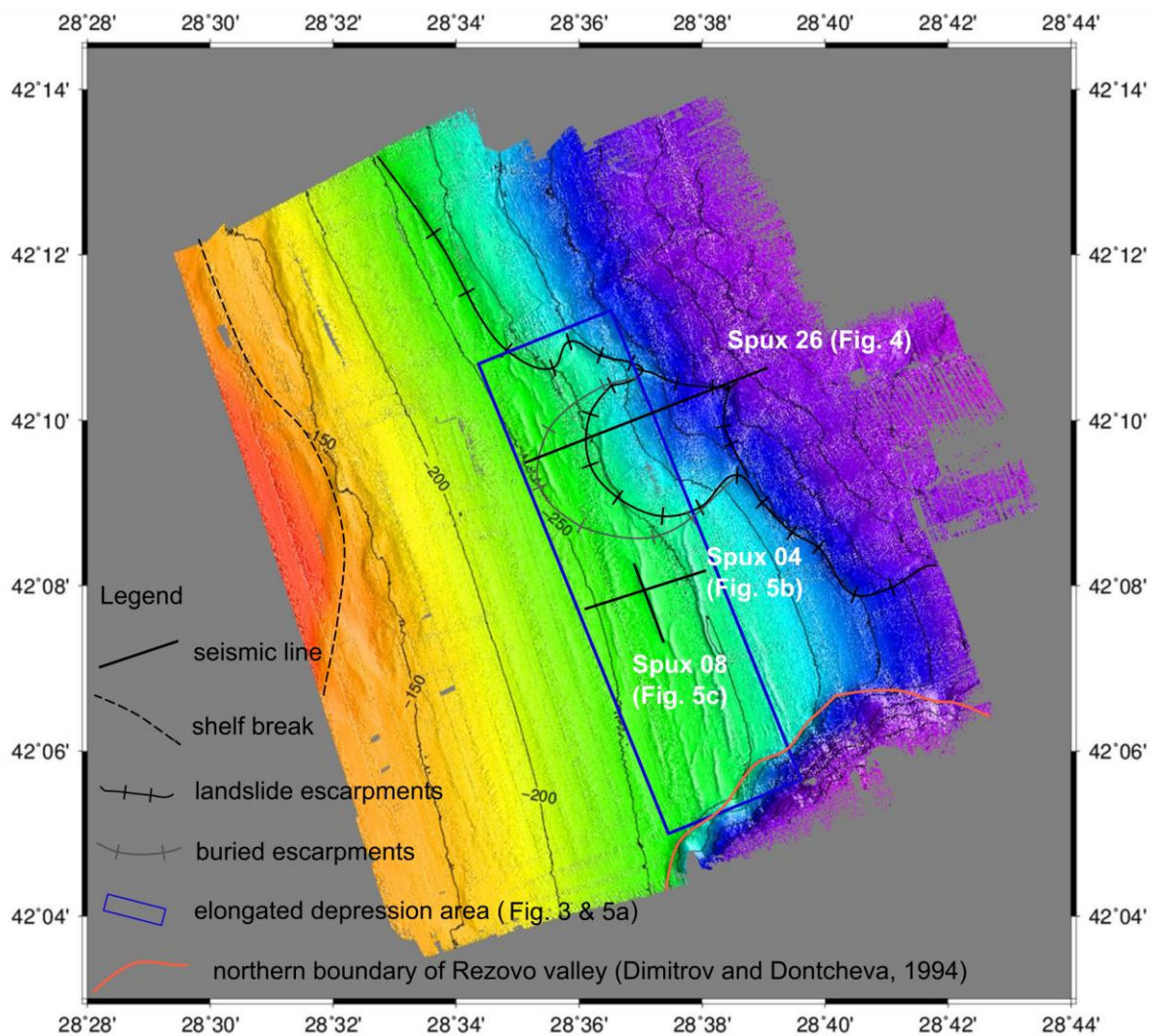
76 More than 230 km<sup>2</sup> of seafloor were mapped with a Reson SeaBat 7111 MBES (100 kHz; 2°  
77 x 1.5° beam angle). The vessel velocity ranged from 3 to 5.2 kn during the surveys. Sound  
78 velocity information was acquired with a real time sound velocity probe near the transducers  
79 (Reson SVP-71). Sound velocity profiles were acquired during CTD casts. The Generic  
80 Mapping Tools (GMT 5.1; Wessel et al., 2013), Fledermaus (Version 7.4; from QPS) and  
81 ArcGIS (Version 10.1) software packages were used to visualize the data. Data processing  
82 was performed with PDS2000.

83 Twenty-eight seismic profiles were acquired using a sparker-streamer combination from  
84 RCMG (Gent University). The Applied Acoustics CSP600 power source (600 Joule) supplied  
85 energy to the sparker ELC820 (100 tips) at a 1.5 s shooting rate. The distance between shot  
86 points was about 2-3 m depending on ship speed. A single-channel streamer with 10  
87 hydrophones was used for signal reception with the IXSEA Delph software (sampling interval  
88 of 100 µs or 125 µs). RadExPro and Seismic Unix were used as processing software,  
89 including smoothing the seafloor horizon by moving average with window size 9 (sea waves  
90 static), Stolt migration (using a constant sound velocity, ~ 1470 m/s) and band pass filtering  
91 (10 - 600 Hz). The Kingdom Suite Software (Version 2015) was used for interpretation and  
92 visualization.

93

### 94 **4. Bathymetry of the study area**

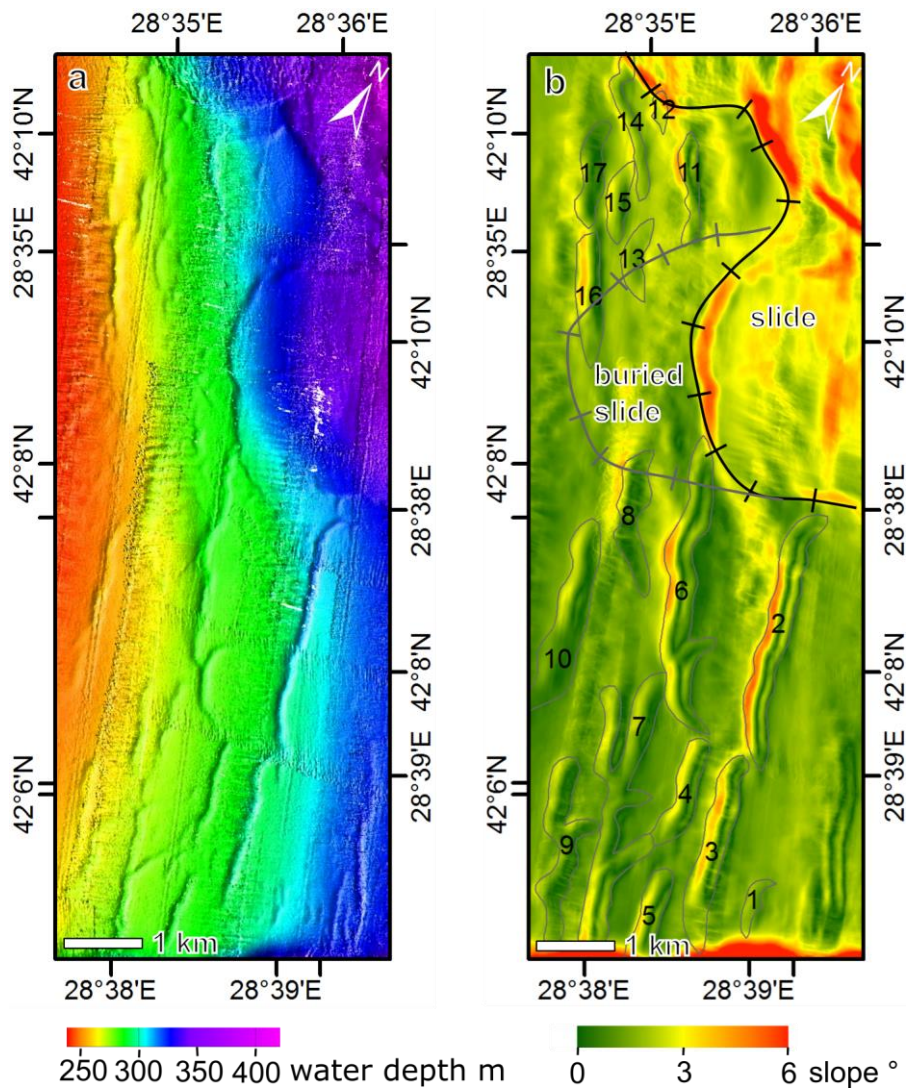
95 The study area is located on the shelf edge and the upper continental slope, with water depths  
96 of 110 to 600 m (Fig. 2). At the shelf break in about 140 m water depth the slope steepens  
97 from 0.5° to 1.2° at the outer shelf edge. The central part of the area shows a gentle terrain  
98 between 140m to 250 m water depths, where the slopes are steeper in the north (~1.8°) than in  
99 the south (1.2°). The eastern part of the area shows a more complex bathymetry. A multiphase  
100 landslide seafloor structure exists in the northeast, creating escarpments along its boundaries  
101 (Fig 2). In the southeast, the seafloor depth increased rapidly by about 400 m (Fig. 2), forming  
102 a valley as a result of the Rezovo fault described by Dimitrov and Dontcheva (1994). Between  
103 this valley and the landslide area, the seafloor appears as a saddle-shaped protrusion without  
104 clear slump features. Upslope of the landslide area and south of it, seventeen elongated  
105 depressions have developed almost parallel to the isobaths between 250 and 300 m water  
106 depth (Fig. 2 & 3).



107  
 108 Fig. 2 Multibeam bathymetry map of the southern Bulgarian slope area, with indications for  
 109 the shelf break, the northern boundary of the Rezovo valley, surface and buried slide  
 110 escarpments as well as elongated depressions. Locations of seismic lines in Fig. 4 and 5 are  
 111 indicated.

112  
 113 The lengths of the depressions range from 540 m to 3720 m and their width varies between  
 114 100 m and 300 m. The depressions are  $< 10$  m deep with an average of  $5.5 \pm 2$  m. Most  
 115 of the depressions are slightly curved, while some are bifurcated (depression #6, 7, 9 and 14;  
 116 Fig. 3). The depressions are asymmetrical, and usually the upper (shallower) flanks have a  
 117 steeper slope ( $2 - 6^\circ$ ) than the lower flanks ( $2 - 4^\circ$ ; Fig. 3b). The elongated depressions can be  
 118 grouped into a southern (depression 1 - 10) and a northern group (depression 11 - 17), with  
 119 landslide escarpments between them. Compared to the southern depressions, the northern  
 120 group depressions are smaller. The average length of depressions in the south (1 - 10) is  $2450$   
 121  $\pm 1000$  m with most of them being 1300 m to 3700 m long. The average length in the north

122 (11 – 17) is only  $1280 \pm 430$  m. The average width and depth of the southern depressions ( $235$   
 123  $\pm 50$  m and  $6.5 \pm 2$  m respectively) are larger than those found in the north ( $200 \pm 50$  m and  $4$   
 124  $\pm 0.8$  m respectively).



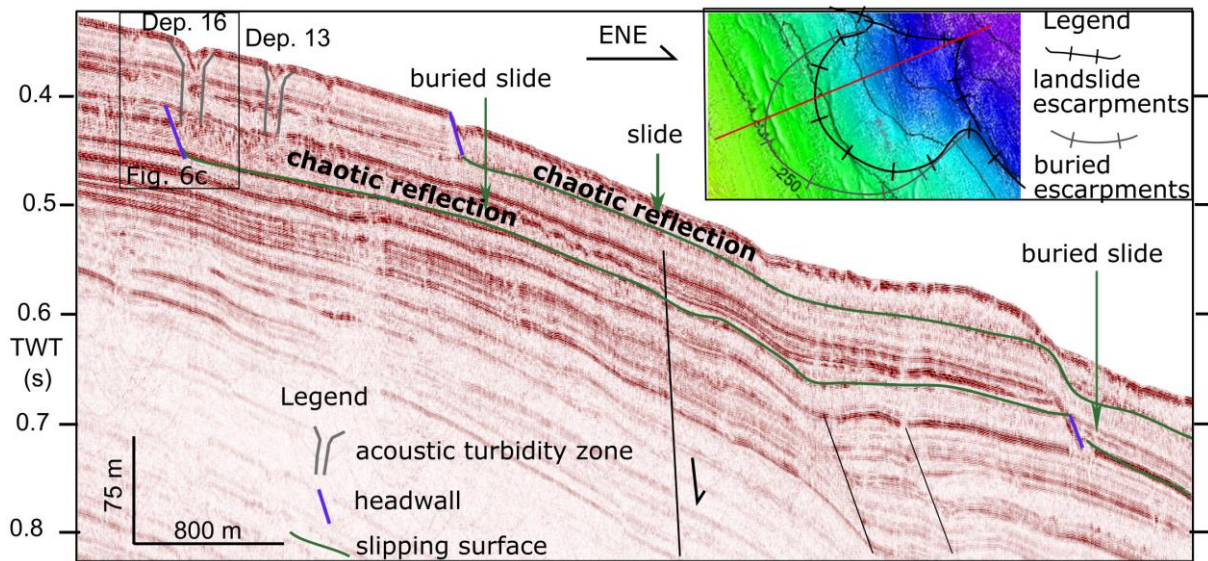
125  
 126 Fig. 3 Bathymetric map (a) and slope map (b) of the elongated depressions area (Fig. 2).  
 127 Depressions are outlined by grey lines and numbered.

128  
 129 **5. Seismic interpretation**

130 The sparker seismic reflection profiles have imaged the sedimentary layers at the uppermost  
 131 150-300 ms of two-way travel time (TWT). In general, the reflectors are subparallel to the  
 132 bathymetry dipping towards the basin in the east. Existing faults do not influence the  
 133 Quaternary deposit structures significantly, except at the southeast part of the study site where  
 134 the Rezovo fault shapes the Rezovo valley (Fig. 2, Dimitrov and Dontcheva, 1994). In the  
 135 northeast, landslides are indicated by escarpments and chaotic reflections in the seismic

136 profiles (Fig. 4). Two slipping surfaces are clearly identified at ca. 90 -110 ms TWT and ca.  
 137 20 - 40 ms TWT below the seafloor. The deeper slipping surface also exists further  
 138 downslope of all seafloor escarpments (indicated by both the grey and black lines in Fig. 2)  
 139 and sedimentary layers above this slipping surface at 40 ms TWT are disturbed. The  
 140 shallower slipping surface is located downslope of the seafloor escarpments (indicated by the  
 141 black line in Fig. 2 and 4). Above this surface, either all sedimentary layers have been  
 142 disturbed up to the seafloor, or the sedimentary layers have been disturbed as well except for  
 143 the top ca. 10 ms TWT of the sediment.

144



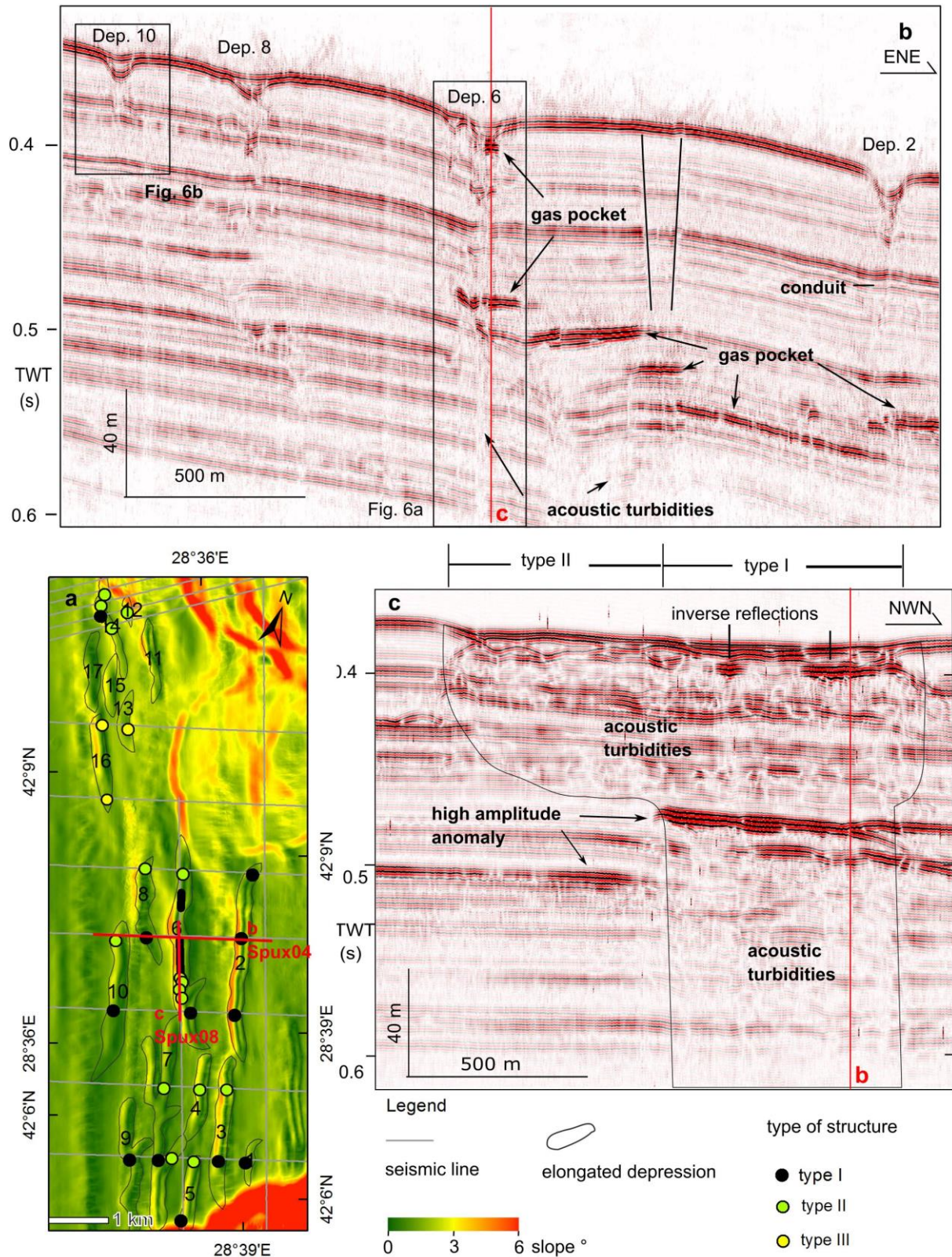
145

146 Fig. 4 The seismic profile Spux 26 (see Fig. 2 for location) shows slides and slide slipping  
 147 surfaces as well as the subsurface structures of the elongated depressions that root at the  
 148 buried slide.

149

150 Vertical acoustic turbidity zones and areas of high amplitudes with reverse polarity (gas  
 151 pockets) which are typical for gas seepage areas can be seen below the depressions (Fig. 5b &  
 152 c). The sub-bottom structure below the elongated depressions varies from one depression to  
 153 the other. It also shows difference in lateral direction within the same depression. These  
 154 differences are related to (1) the depths of the acoustic turbidity under the depressions, (2) the  
 155 appearance of gas pockets, (3) the position of possible related landslides. Based on these  
 156 differences, we classified the sub-bottom structures beneath the elongated depressions into  
 157 three types, with a summary shown in Fig. 5a, and typical examples shown enlarged in Fig. 6.

158



159

160

161

162

Fig. 5 (a) Overview of the three types of sub-surface structures under the depressions. Seismic line Spux 04 (b) runs perpendicular to depression 6 and Spux 08 (c) runs along its axis, showing the varying distribution of acoustic turbidity zones and gas pockets.



163 *Type I—gas focusing conduits*

164 For one set of depressions several seismic profiles show that the lower limit of the acoustic  
165 turbidity zone exceeds the recording depth of the sparker data ( $> 200$  ms TWT below the  
166 seafloor, Fig. 6a). At least one profile of each depression in the southern group shows an  
167 acoustic turbidity zone deeper than 200 ms TWT below the seafloor, while only one profile  
168 shows a deep rooted acoustic turbidity zone underneath a depression in the north (Fig. 5a).  
169 Seismic profiles that lie perpendicular to the elongated depressions image a narrow acoustic  
170 turbidity zones (Fig. 5b), but show an acoustic turbidity zone at least 700 m long in profile  
171 Spux 08 that runs along depression 6 (Fig. 5c). This indicates that the acoustic turbidity zones  
172 are narrow cuboid volumes and not cylindrical isolated chimneys. These acoustic turbidity  
173 zones reach deeper than both slipping surfaces of landslides. Sedimentary layers on the two  
174 sides of the acoustic turbidity zones do not show a significant dislocation. In the area beneath  
175 the elongated depressions, gas pockets are common along the acoustic turbidity zones.

176

177 *Type II—shallow rooted structure without gas pockets*

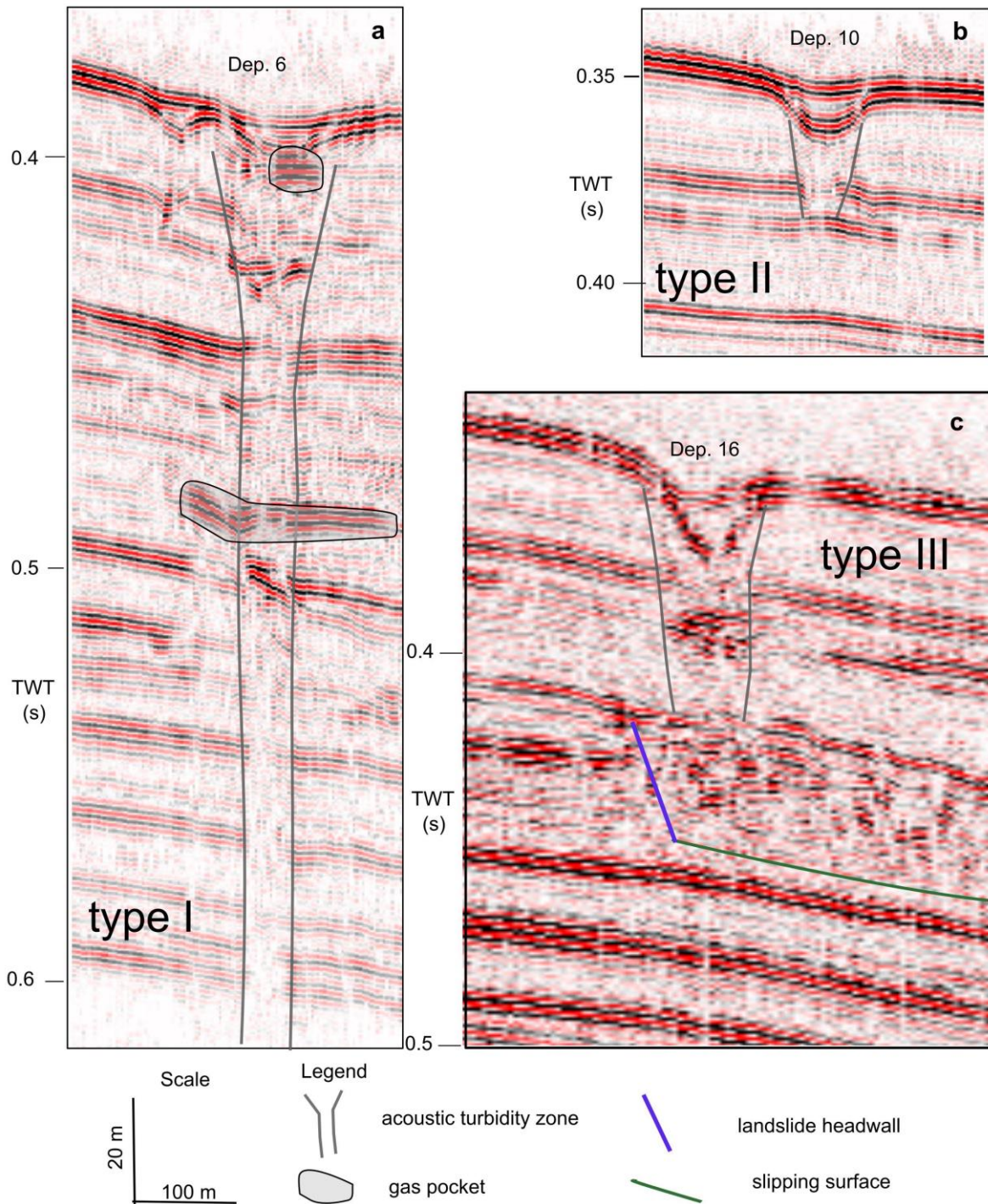
178 In other seismic profiles the lower boundary of the acoustic turbidity zones could be imaged  
179 at 70 ms TWT below the seafloor (Fig. 6b). These acoustic turbidity zones cover the depth  
180 interval of the landslides. The sedimentary layers on both sides of the acoustic turbidity zones  
181 do not show a significant dislocation, and gas pockets are not found in these profiles.

182

183 *Type III—structure rooted in the re-deposited landslides*

184 The acoustic turbidity zones under depression 13 and 16 link to re-deposited sediments of  
185 buried landslides. The acoustic turbidity zones under depression 13 link to the chaotic  
186 reflections of a buried slide (Fig. 4), while turbidity areas under depression 16 just occur  
187 above the headwall of the slide (Fig. 4 & 6c). The acoustic turbidity zones root in the chaotic  
188 reflections of landslides, and do not penetrate the slipping surface.

189



190

191 Fig. 6 The seismic profiles show three kinds of typical structures under the depressions. (a) type I --  
 192 the acoustic turbidity zone roots deeper than 200 ms TWT below the seafloor, and gas pockets are  
 193 found. (b) type II -- the acoustic turbidity zone roots shallower than 30 ms TWT below the seafloor,  
 194 and there are not gas pockets. (c) type III -- the acoustic turbidity zone roots in the buried landslides.

195 See Fig. 5b for locations of profiles a and b, see Fig. 4 for location of profile c.

196

## 197 **6. Discussion**

198 The close proximity of landslides with elongated depressions and the presence of shallow gas  
199 pockets underneath these depressions imply that their location and formation results from a  
200 combined effect of slope instability and gas migration/seepage. Seafloor pockmarks have  
201 often been interpreted as indicators for (past) fluid/gas seepage and in some circumstances  
202 they have been found adjacent to and often upslope of landslides (Hovland et al., 2002).  
203 Typical examples are the Storegga Slide area at Nyegga, offshore mid-Norway (Reiche et al.,  
204 2011), the Baiyun Slide on the northern slope of the South China Sea (Li et al., 2014), the  
205 NG1 slide area in the north-east Atlantic (Riboulot et al., 2013), the Humboldt Slide offshore  
206 California (Yun et al., 1999) or the Albemarle Currituck slide area at the U.S. Atlantic margin  
207 (Hill et al., 2004; Newman et al., 2008). Çifçi et al. (2003) proposed that elongated depressions  
208 (described by the authors as pockmarks) in the Turkish shelf of the Black Sea formed by the  
209 merging of circular pockmarks. However, most of the depressions in our survey area are  
210 kilometer scale, elongate features. Smaller circular pockmarks are not present in the research  
211 area (Fig. 2). Although a few depressions are slightly curved or bifurcate, the walls of the  
212 depressions are straight in general (Fig. 3). There is no clear evidence that individual circular  
213 pockmarks have been developed and thus the assumption that small circular pockmarks  
214 merged into elongated depressions seems unreasonable for the discussed research area.

215 Hill et al. (2004) and Newman et al. (2008) suggested that the elongated asymmetric  
216 depressions along the U.S. Atlantic margin (termed “gas blowouts”) formed primarily by gas  
217 expulsion due to tensional stress, and the related downslope creep of sediments is linked to  
218 gas release along the seafloor of the shelf edge. The depression shapes in our research area are  
219 highly elongated and asymmetric (Fig. 3), showing similar shapes as those along the U.S.  
220 Atlantic margin. Along the Bulgarian slope research area, gas pockets are found along the  
221 acoustic turbidity zones which root deeper than the recording depth of the sparker data (Fig. 5  
222 & 6a), implying these turbidity zones (type I structure) are the main conduit for fluid  
223 migration. As the sedimentary layers on both sides of the acoustic turbidity zones do not show  
224 a significant dislocation, they are not formed by Quaternary faults (Fig. 5). These acoustic  
225 turbidity zones ( $> 200$  ms TWT below the seafloor, Fig. 6a) reach deeper than the two  
226 detected slipping surfaces (Fig. 4), ruling out the possibility that they are formed by  
227 sedimentary instabilities that are related to sediment movement/landslides (Chapron et al.,  
228 2004; Baeten et al., 2013; Laberg et al., 2013). We suggest that these vertical acoustic

229 turbidity zones are primarily fractured by gas migration and then serve as conduits for  
230 following gas.

231 In contrast to many other more focused and round/oval ‘gas chimneys’, the gas conduits  
232 offshore Bulgaria have a more continuous wall-like shape that follows the elongated  
233 depressions at the seafloor surface (Fig. 5). The length of these gas-conduit walls can be  
234 laterally shorter than the depressions above. The wall-like shape of the conduits points to a  
235 tensional stress regime within the Quaternary sediments and they are present under each  
236 depression in the southern part of the working area (depression 1 to 10). In contrast, only one  
237 has been found under the northern group of depressions (depression 11-17). We interpret this  
238 as an artifact created by the limited coverage of seismic lines in the north (Fig. 5a). We thus  
239 suggest that the buoyancy induced gas migration through the sediment is responsible for the  
240 formation of the type I structure under the depressions, and that this controlled the location of  
241 the seafloor elongated depressions.

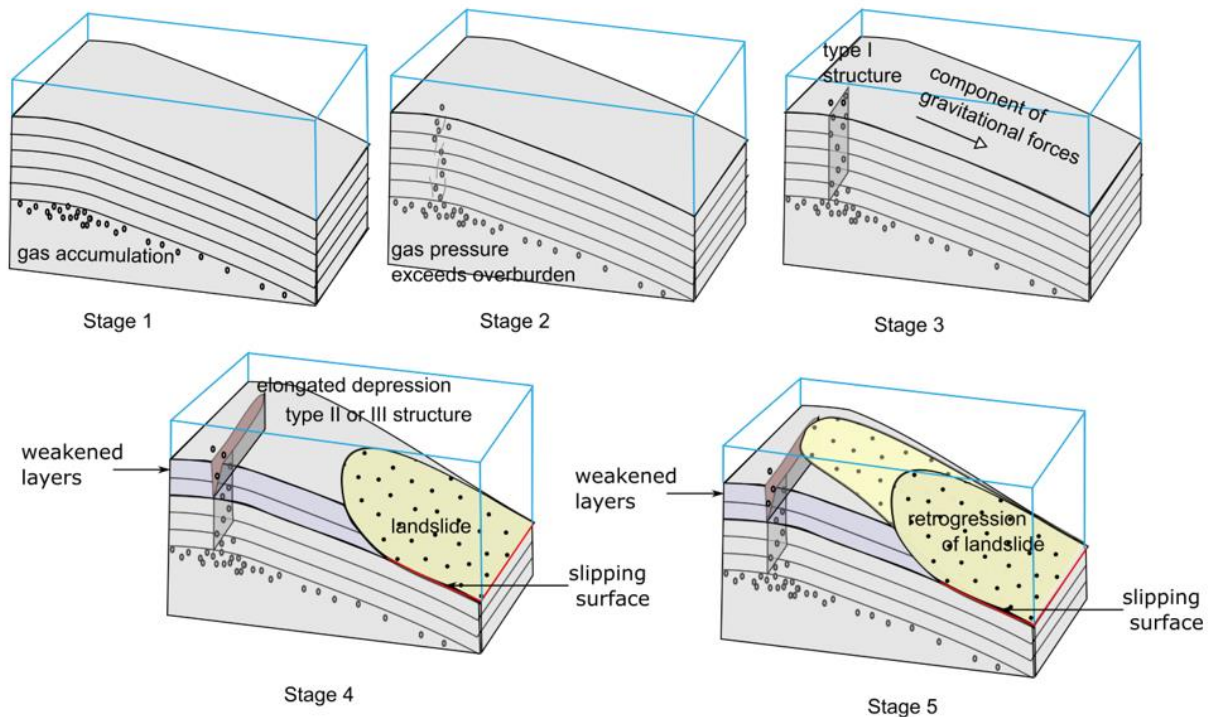
242 Considering only the process of gas migration as the reason for the depression formation is  
243 not comprehensive. This is because gas pockets are not found along type II and type III  
244 structures (Fig. 5a, 6b & c), which indicates that gas migration and trapping is/has been absent  
245 under some parts of the elongated depressions. Secondly, downslope sediment creeping,  
246 which is proposed to contribute shaping the feature of the “gas blowouts” along the U.S.  
247 Atlantic margin (Hill et al., 2004), is not found in our research area.

248 Tension fractures, which are regarded as the initial stages of slope failure (Driscoll et al.,  
249 2000; Reiche et al., 2011; Laberg et al., 2013; Greene et al., 2006; Baeten et al., 2013), are  
250 assumed to lengthen and shape the elongated depressions. Under some of them, acoustic  
251 turbidity zones occur in the same shallow depth down to 70 ms TWT below the seafloor (type  
252 II & III structures) and indications of landslides could be observed. This might implicate that  
253 the sedimentary slipping at this depth interval may have an influence on the formation of  
254 these acoustic turbidity zones, and thus the elongated shape of the seafloor depressions.  
255 Landslides accompanied by tension fractures have also been found in several other  
256 continental margins. For example, the extension of landslide headwalls as fractures, such as  
257 the cracks in the Santa Barbara Channel (Greene et al., 2006), has been confirmed by 3-D  
258 modelling to be shear fractures as described by Martel (2004). Cracks of the Norwegian  
259 continental slope (Laberg et al., 2013; Baeten et al., 2013) have been described at the upslope  
260 of landslide headwalls and were interpreted to be the result of tension fractures. Tension  
261 fractures are usually distributed en échelon as surficial expression (Laberg et al., 2013), while

262 the depressions in our study area are subparallel linear. The difference may be because of the  
263 influence of gas migration along the type I structure or the saddle-shaped seafloor (Fig. 2)  
264 on the stress distribution.

265 As a conceptual model, the following sequential stages of bubble migration, gas accumulation,  
266 sediment weakening and sediment sliding are considered as a likely process for the formation  
267 of the elongated depressions on the upper Bulgarian slope. With the accumulation of gas  
268 under impermeable sedimentary layers, especially in the area where the slope of the seafloor  
269 increases seaward (Fig. 7 stage 1), pore pressure increases initiating the breakthrough of gas  
270 bubbles at individual locations, a process similar to the formation of gas chimneys (Fig. 7  
271 stage 2). The vertical weakening of the sediment due to buoyancy driven gas bubble migration  
272 that fractures the sediment define the upper border of subsequent mass movement, but also the  
273 location and orientation of the elongated depressions. Near the gas-weakened conduit(s), the  
274 potential of gravitational forces to cause fracturing is highest, and these areas may turn into a  
275 growing gas migration plane in parallel to the slope. This will develop over time in the  
276 observed acoustic turbid 'conduit wall' with gas pockets (Fig. 7 stage 3, e.g. the type I  
277 structure in Fig. 5c). In stage 4, tension fractures may either occur together with landslides  
278 during one mass movement event, or form when the support from downslope or underneath  
279 sedimentary layers weakens. The areas upslope of landslide, the lateral/slope parallel  
280 extension of landslide headwalls and sedimentary layers above buried landslides are the most  
281 likely positions for the development of tension fractures. Areas with already weakened  
282 sediment structures as the 'conduit walls' give priority to a further development of tensional  
283 fractures/cracks causing that acoustic turbidity zones in shallow sedimentary layers are  
284 lengthened and widened (e.g. the type II structure in Fig. 5c), creating asymmetric elongated  
285 depressions on the seafloor (Fig. 7 stage 4). In stage 5, the elongated depression and the  
286 underneath 'conduit wall' or tensional cracks might transform into headwalls of sliding sites,  
287 facilitating the upslope retrogression of mass movement. One of those headwalls forms a  
288 slope-parallel extension of the depression developed in the north of depression 6 (Fig. 3b).

289



290

291 Fig. 7 Schematic outlining the formation process of elongated depressions. See text for explanation.

292

## 293 7 Conclusions

294 The series of asymmetric elongated depressions, imaged in seismic and multibeam-echo  
 295 sounder data show a very close relation with gas migration and sediment sliding in the upper  
 296 continental slope offshore southern Bulgaria. The lengths of the depressions range from 540  
 297 m to 3720 m, the widths vary between 100 m to 300 m, and their depths are < 10 m. Three  
 298 types of vertical acoustic turbidity zones are found below the elongated depressions, including  
 299 gas focus conduits that rooted deeper than the recording depth of the sparker data, shallow  
 300 rooted structure without gas pockets, and structure rooted in the re-deposited landslides. The  
 301 data imply that no faults existed prior to the onset of vertical gas migrations. However, once  
 302 gas bubble migration started to weaken the sediments vertically and laterally, slope-parallel  
 303 fracturing began to evolve. When the buoyancy of gas-charged fluids exceeds the overburden  
 304 pressure, fluids and gas expelled through the overlying sediments, creating gas focusing  
 305 conduits. At the depth interval of sediment sliding, conduits are lengthened and widened,  
 306 developing into tensional fractures or cracks and so pre-defining/shaping the elongated  
 307 depressions on the seafloor. The weakened surface sediments in the depressions are prone to  
 308 be eroded by bottom currents which further help to deepen and widen these depressions until  
 309 the observed stage.

310 **Acknowledgements**

311 We acknowledge the captains, the crew and technicians of the R/V Akademik for all support  
312 during the SPUX cruise in 2012. The cruise SPUX (AK211) has been funded by the European  
313 project EUROFLEETS (Seventh Framework Programme, grant agreement No. 228344)  
314 through transnational access to the research vessel “RV Akademik” operated by the Institute  
315 of Oceanology Bulgarian Academy of Science (Bulgaria). We thank Timo Zander, Peter  
316 Urban from GEOMAR for introductions to the Kingdom Suit software, and Linux  
317 programming, and Wei Li (from Kiel University) for seismic interpretation. We very much  
318 appreciated the comments of Prof. Marc De Batist from Gent University and two anonymous  
319 reviewers on an earlier version of this paper. We also thank Inken Preuss and Edna Hütten  
320 who were a great help in sorting out the English. This is publication 27 of the DeepSea  
321 Monitoring group at GEOMAR.

322

323 **References**

- 324 Baeten, N.J., Sverre, J., Forwick, M., Vorren, T.O., Vanneste, M., Fredrik, C., Kvalstad, T.J.,  
325 Ivanov, M., 2013. Geomorphology Morphology and origin of smaller-scale mass  
326 movements on the continental slope off northern Norway. *Geomorphology* 187, 122–134.  
327 doi:10.1016/j.geomorph.2013.01.008
- 328 Bøe, R., Rise, L., Ottesen, D., 1998. Elongate depressions on the southern slope of the  
329 Norwegian Trench (Skagerrak): Morphology and evolution. *Marine Geology* 146, 191–  
330 203. doi:10.1016/S0025-3227(97)00133-3
- 331 Chapron, E., Van Rensbergen, P., De Batist, M., Beck, C., Henriët, J.P., 2004. Fluid-escape  
332 features as a precursor of a large sublacustrine sediment slide in Lake Le Bourget, NW  
333 Alps, France. *Terra Nova* 16, 305–311. doi:10.1111/j.1365-3121.2004.00566.x
- 334 Çifçi, G., Dondurur, D., Ergün, M., 2003. Deep and shallow structures of large pockmarks in  
335 the Turkish shelf, Eastern Black Sea. *Geo-Marine Letters* 23, 311–322.  
336 doi:10.1007/s00367-003-0138-x
- 337 Dimitrov, L., Dontcheva, V., 1994. Seabed pockmarks in the southern Bulgarian Black Sea  
338 Zone. *Bulletin of the Geological Society of Denmark* 41, 24–33.
- 339 Driscoll, N.W., Weissel, J.K., Goff, J. a., 2000. Potential for large-scale submarine slope  
340 failure and tsunami generation along the U.S. mid-Atlantic coast. *Geology* 28, 407–410.  
341 doi:10.1130/0091-7613(2000)28<407: PFLSSF>2.0.CO;2
- 342 Genov, I., Dimitrov, O., 2003. Faults and Fault Activity Determined on the Basis of Seismic

343 Stratigraphy in the Region East from the West-Ahtopol Rise - Southern. *Comptes*  
344 *Rendus De Lacademie Bulgare Des Sciences* 56, 71. doi:10.1007/s13398-014-0173-7.2  
345 Georgiev, G., 2012. Geology and Hydrocarbon Systems in the Western Black Sea. *Turkish*  
346 *Journal of Earthences* 21, 723–754. doi:10.3906/yer-1102-4  
347 Greene, H.G., Murai, L.Y., Watts, P., Maher, N. a., Fisher, M. a., Paull, C.E., Eichhubl, P.,  
348 2006. Submarine landslides in the Santa Barbara Channel as potential tsunami sources.  
349 *Natural Hazards & Earth System Sciences* 6, 63–88. doi:10.5194/nhess-6-63-2006  
350 Hill, J.C., Driscoll, N.W., Weissel, J.K., Goff, J. a., 2004. Large-scale elongated gas blowouts  
351 along the U.S. Atlantic margin. *Journal of Geophysical Research Atmospheres: Solid*  
352 *Earth* 109, B09101. doi:10.1029/2004JB002969  
353 Hovland, M., Gardner, J. V., Judd, a. G., 2002. The significance of pockmarks to  
354 understanding fluid flow processes and geohazards. *Geofluids* 2, 127–136.  
355 doi:10.1046/j.1468-8123.2002.00028.x  
356 Laberg, J.S., Baeten, N.J., Lågstad, P., Forwick, M., Vorren, T.O., 2013. Formation of a large  
357 submarine crack during the final stage of retrogressive mass wasting on the continental  
358 slope offshore northern Norway. *Marine Geology* 346, 73–78.  
359 doi:10.1016/j.margeo.2013.08.008  
360 Li, W., Wu, S., Wang, X., Zhao, F., Wang, D., Mi, L., Li, Q., 2014. Baiyun Slide and Its  
361 Relation to Fluid Migration in the Northern Slope of Southern China Sea, in: Krastel, S.,  
362 Behrmann, J.-H., Völker, D., Stipp, M., Berndt, C., Urgeles, R., Chaytor, J., Huhn, K.,  
363 Strasser, M., Harbitz, C.B. (Eds.), 6th International Symposium on Submarine Mass  
364 Movements and Their Consequences, *Advances in Natural and Technological Hazards*  
365 *Research*. Springer International Publishing, Cham, pp. 105–115. doi:10.1007/978-3-  
366 319-00972-8\_10  
367 Martel, S.J., 2004. Mechanics of landslide initiation as a shear fracture phenomenon. *Marine*  
368 *Geology* 203, 319–339. doi:10.1016/S0025-3227(03)00313-X  
369 Mienert, J., Vanneste, M., Haflidason, H., Bünz, S., 2010. Norwegian margin outer shelf  
370 cracking: a consequence of climate-induced gas hydrate dissociation? *International*  
371 *Journal of Earth Sciences* 99, 207–225. doi:10.1007/s00531-010-0536-z  
372 Newman, K.R., Cormier, M.H., Weissel, J.K., Driscoll, N.W., Kastner, M., Solomon, E. a.,  
373 Robertson, G., Hill, J.C., Singh, H., Camilli, R., Eustice, R., 2008. Active methane  
374 venting observed at giant pockmarks along the U.S. mid-Atlantic shelf break. *Earth &*  
375 *Planetary Science Letters* 267, 341–352. doi:10.1016/j.epsl.2007.11.053



376 Pilcher, R., Argent, J., 2007. Mega-pockmarks and linear pockmark trains on the West  
377 African continental margin. *Marine Geology* 244, 15–32.  
378 doi:10.1016/j.margeo.2007.05.002

379 Reiche, S., Hjelstuen, B.O., Haflidason, H., 2011. High-resolution seismic stratigraphy,  
380 sedimentary processes and the origin of seabed cracks and pockmarks at Nyegga, mid-  
381 Norwegian margin. *Marine Geology* 284, 28–39. doi:10.1016/j.margeo.2011.03.006

382 Riboulot, V., Cattaneo, a., Sultan, N., Garziglia, S., Ker, S., Imbert, P., Voisset, M., 2013.  
383 Sea-level change and free gas occurrence influencing a submarine landslide and  
384 pockmark formation and distribution in deepwater Nigeria. *Earth & Planetary Science*  
385 *Letters* 375, 78–91. doi:10.1016/j.epsl.2013.05.013

386 Ross, D.A., 1978. *Black Sea Stratigraphy*. Initial Report of the Deep Sea Drilling Project, vol.  
387 42, 2. US Government Printing Office, Washington DC. 17–26.

388 Wessel, P., Smith, W.H.F., Scharroo, R., Luis, J., Wobbe, F., 2013. Generic Mapping Tools:  
389 Improved Version Released. *Eos Transactions American Geophysical Union* 94, 409–  
390 410. doi:10.1002/2013EO450001

391 Yun, J.W., Orange, D.L., Field, M.E., 1999. Subsurface gas offshore of northern California  
392 and its link to submarine geomorphology. *Marine Geology* 154, 357–368.  
393 doi:10.1016/S0025-3227(98)00123-6